We are IntechOpen, the world's leading publisher of Open Access books Built by scientists, for scientists

4,800
Open access books available

122,000
International authors and editors

135M
Downloads

Our authors are among the

154
Countries delivered to

TOP 1%
most cited scientists

12.2%
Contributors from top 500 universities

CLARIVATE ANALYTICS BOOK CITATION INDEX INDEXED

WEB OF SCIENCE™

Selection of our books indexed in the Book Citation Index in Web of Science™ Core Collection (BKCI)

Interested in publishing with us?
Contact book.department@intechopen.com

Numbers displayed above are based on latest data collected.
For more information visit www.intechopen.com

Chapter

Large Molecule Fragmentation Dynamics Using Delayed Extraction Time-of-Flight Mass Spectroscopy

Najeeb Punnakayathil

Abstract

A time-of-flight mass spectrometer with a pulsed electron beam, delayed and pulsed extraction of the recoil ion is reported. This new technique is named as Delayed Extraction Time of Flight Mass Spectrometer (DEToF). The effectiveness of this technique is highlighted by studying the statistical decay of mono-cations over microsecond timescales from large molecules. Various details of the design and operation are performed in the context of electron impact ionization and fragmentation of few PAHs, naphthalene ($C_{10}H_8$), quinoline (C_9H_8N) and it isomer Isoquinoline (C_9H_8N) and are used as a test bench mark for large molecules fragmentation dynamics using DEToF. In this chapter we discuss the fragmentation dynamics of Naphthalene molecule and time evolution of various fragmentation channels of these PAH, explored using a rapid but delayed extraction of recoil ions. The temporal behavior of acetylene (C_2H_2), HCN, diacetylene (C_4H_2) and C_2H_2+HCN loss are observed and compared with the associated Arrhenius decay constant, internal energy and plasmon excitation energy.

Keywords: large molecule spectroscopy, delayed extraction time of flight, PAHs

1. Introduction

Large molecules in general and in particular, polycyclic aromatic hydrocarbons (PAHs) are found in the terrestrial environment as well as in the interstellar medium abundantly [1]. They are primarily formed on earth by the incomplete combustion of organic molecules. The origin of Diffuse Interstellar Bands (DIBs), that are absorption features seen in the spectra of astronomical objects in optical and infrared wavelengths has been attributed to PAHs [2]. Considering the abundance of high energy radiation in the interstellar medium, it remains an interesting endeavor to understand the mechanism behind the survivability of PAHs in such environments. Because of such astronomical significance, the interaction of PAHs with photons and charged particles has seen renewed interest in the last couple of decades. Even in recent times, several results have been reported globally on the topic of ion-PAH collisions [3–6]. In addition, detailed experiments are being carried out using synchrotron radiation sources [7]. High energy electron interaction

with PAHs, on the other hand, has not been investigated in the context of radiation tolerance of PAHs.

High energy photon impact studies are often made using synchrotron radiation sources [8–10] with atoms or molecules as targets. Such mass spectrometric techniques along with the secondary electron selectivity methods like photoelectron-photoion coincidence (PEPICO) spectroscopy and threshold photoelectron-photoion coincidence (T-PEPICO) spectroscopy helps in determining the appearance energy and time scales of various dissociation channels of molecules very accurately. By modeling the line shape of the mass spectrum that arises due to slow decay, corresponding decay constant can be measured for microsecond range [11]. Longer decay times are probed using ion traps with variable extraction time [12]. It is essential to note that the excitation mechanism in conjunction with the appropriate electron spectrometer gives a very narrow range of internal energy left in the molecule. In particular, near the threshold, the internal energy is generally larger than the original thermal energy of the molecule, leading to resulting decay constants also range in a narrow band of values. Considering that the Arrhenius law decay rates are extremely sensitive to the internal energy, this factor very importantly implies that the decay rates with such secondary electron gated species will lie in a narrow range. Charged particle interaction with molecules will have a much broader range of internal energies and a precise value of decay constant cannot be obtained even with a suitable secondary electron energy gating. Hence modeling of exact decay curve for charged particle collision induced dissociation is deemed impractical. Moreover often minor fragmented peaks will interfere with the tail of mass spectrum due to isotopic effects or due to the presence of many hydrogen atoms in the molecule.

Electron impact ionization is one of the oldest mass spectrometric tools but it mainly focuses on identifying the possible ionization and fragmentation channels particularly between 70 and 100 eV energy. Typically, the mass spectrometric data available in the database is taken in this range, because ionization cross-section normally peaks in this region [13]. In past, several electron impact ionization investigations have been done mainly on inert gasses, diatomic or triatomic molecular gasses. Several experiments and modeling attempts have been made for such studies with electron energy up to few keV [14–16]. But such studies are very rare for larger molecules; the main reason is the complexity of a large number of decay channels, difficulties in separating indirect from direct ionization processes. For large molecules there are few attempts have been made in some specific cases for target specific energy loss modeling within the charged particle interaction with molecules [17].

The stability of PAHs during the interaction of charged particles, cosmic rays and photon sources in the interstellar medium is of our interest [4, 7]. It has been shown conclusively that for charged particle interaction with naphthalene, the plasmon excitation is a major channel particularly at high velocities of projectile wherein the other processes have diminishing cross section [4]. It is also seen that acetylene (C_2H_2) loss comes as a by-product of such plasmon excitation with a very specific range of decay constants. We use naphthalene as a model since it exhibits many general spectroscopic and structural properties of larger PAHs [18]. An attempt is made to investigate the interaction of high energy electron beam with PAHs and assess the time dependence of C_2H_2 evaporation in comparison with the other channels using a Time-of-Flight (ToF) mass spectrometer. Recent studies on benzene using PEPICO highlight the importance of the time variation of the decay channel [11]. We explore the time evolution of various decay channels within the first 5 μs of naphthalene ionization. This is achieved by the correlated pulsing of the electron source and recoil ion extraction field. We specifically target C_2H_2 and

diacetylene (C_4H_2) evaporation process to identify the influence of plasmon excitation at different electron beam energies up to 1 keV.

The pulsed extraction of ions in a ToF setup can be used to analyze the evolution of a time-dependent population of various fragmentation channels. If the decay constants are in the range of $10^5 \sim 10^6$, then the thermal velocity dispersion does not affect the collection efficiency if it becomes possible to probe the system within sufficient time. Even though such a unique system has limited applicability, it has helped in our present investigation to study the evaporative loss from a PAH molecule due to electron impact and the decay rate for acetylene and diacetylene loss in naphthalene has been shown to have decay constant in the range of $10^5 \sim 10^6$ sec^{-1} at 8–9 eV internal energy [12, 18]. So, the decay time of acetylene and diacetylene is of the order of 1–10 μs. The ionization potential of naphthalene is 8.12 eV [19] and the plasmon resonance of naphthalene is observed at 17 eV [4]. The instrumentation presented here is very effective under such conditions.

2. Experimental set-up

For detection of product ions we use a Wiley-McLaren type time-of-flight mass spectrometer [20] with the pulsed extraction technique. The experimental set-up with the data acquisition system is shown in **Figure 1**. This experimental set-up consists of pusher (labeled as P_1 in **Figure 1**) as well as puller (labeled as P_2 in **Figure 1**) plates of thickness 1 mm and outer diameter of 105 mm and the puller plate has an opening diameter of 26 mm and for field uniformity that is covered with a nickel mesh characterized by 40 lines per inch, which allows a transmission efficiency of 95% of the molecular ions. For the field-free drift of ions, we have a drift tube of length 200 mm with an opening of 25 mm covered by a nickel mesh for field uniformity. Between pusher (P_1) and puller plates (P_2) there is 16 mm gap while that between the puller and the drift tube is 5 mm. A low current – high energy (1–5 keV) electron gun is used for ionizing the target molecule, which is custom made using CRT tube. Electron gun produces electron from filament via thermionic emission with a current of typically about 180 mA. There are two sets of

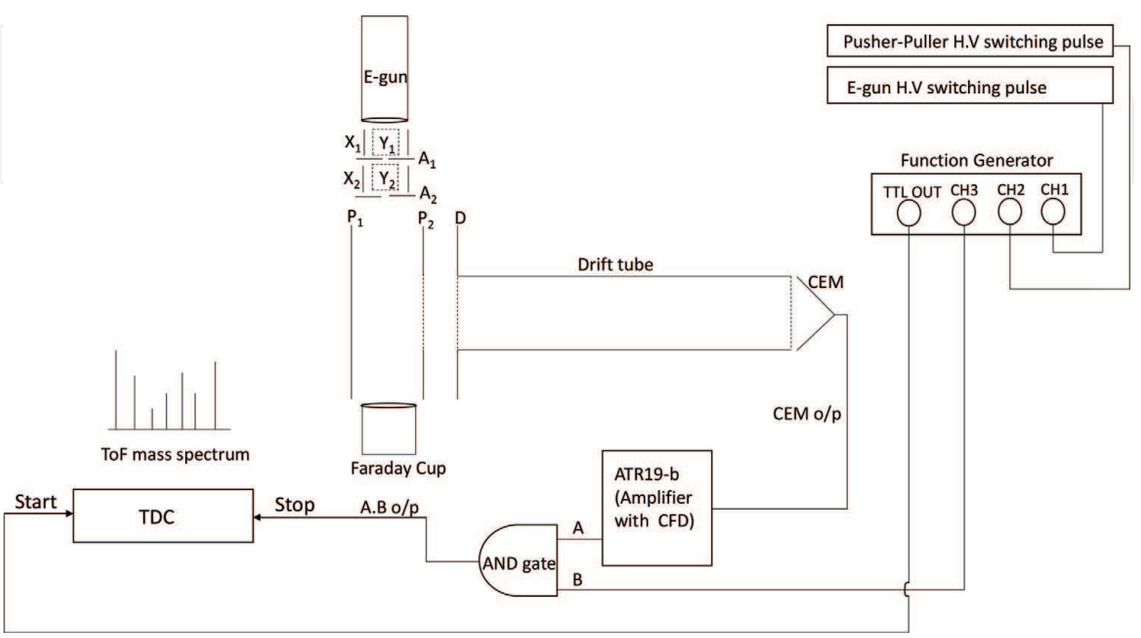

Figure 1.
The developed experimental set-up.

positional X-Y deflectors mounted after the focusing lens and two apertures (A_1, A_2), one between the two deflector sets (A_1) and the other after the deflectors (A_2), to discriminate the secondary electrons from the internal scattering of the beam. The whole electron gun assembly is floated, which voltage is decides the electron beam energy. A pulsed switch with a variable ON time width is used to operate the electron gun. For pulsed extraction ToF, a high voltage in the push-pull mode with a 50 ns rise and fall time is used which is a home-built high voltage MOSFET switch. A cylindrical Faraday cup made from stainless steel (SS-304), of length 100 mm and radius 25 mm to collect electron beam. This Faraday cup is placed at a distance of 50 mm from the exit of the interaction region. The Faraday cup is biased to +36 V using batteries to collect projectile electrons as well as the secondary electrons produced by the primary beam due to collision with Faraday cup wall. The intended target molecule is introduced into the interaction zone that is well localized in space through a fine capillary of internal diameter 300 microns and length of 15 mm. To avoid any possible secondary electron emission due to the electron beam colliding with the capillary, the capillary exit is kept nearly 5 mm away from the center of the ToF interaction region. A channel electron multiplier (CEM) is used for the detection of molecular ions, which is biased to a voltage of −2600 V. The electron gun, the pusher and puller plates are pulsed as per our pulsing sequence for delayed time-of-flight mass spectrometry as shown in **Figure 2**. Molecular ions produced due to electron impact (in the well-focused interaction region) are accelerated by the electric field and compensated for the special spread in the second region before entering the field-free drift tube followed by the ion detector. A multi-hit time-to-digital converter [Agilent TDC (Model: U1051A)] is employed as part of data acquisition system. To filter out the noises picked up by the detector due to switching pulses, we use a desired gate pulse.

Stainless steel (SS – 304) high vacuum chamber with metal joints are used to place the whole experimental setup. For better alignment, the time-of-flight mass spectrometer is mounted along the axis of the chamber and electron gun in perpendicular to its axis which ensure the cross beam (perpendicular) interaction of projectile beam and the molecular jet. There are several auxiliary ports for pumping, electrical connections and vacuum gauges. The whole chamber is pumped by two

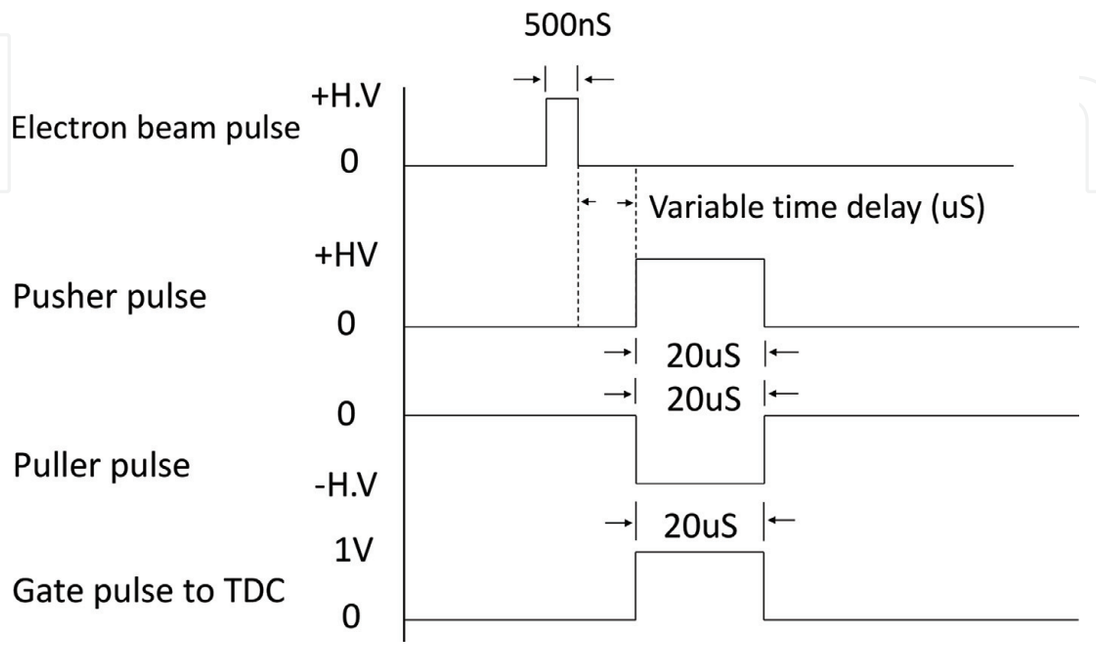

Figure 2.
Pulsing sequence used for delayed extraction time-of-flight mass spectrum.

turbo molecular vacuum pumps backed by a rotary pump. The pressure of the chamber goes down to 5.8×10^{-8} mbar, that rises up to a maximum of 5.0×10^{-7} mbar with the target gas. With naphthalene as the target, no heating was required due to the relatively large vapor pressure at 300 K. With the naphthalene target (has a purity greater than 98 %), the chamber pressure was maintained at $\sim 3.0 \times 10^{-7}$ mbar.

3. High voltage MOSFET switch

Electron beams are very sensitive to electrode voltages and hence in a time of flight spectrometer used in electron impact studies, they need special arrangement to limit the effect of the extraction voltages on the pusher and puller. Usually, this can be achieved by pulsing the extraction voltages. Switching noise pickup on the detector channels are the major complications with this arrangement. The electron beam cannot be allowed to persist during the extraction process, failing to which the beam might cause a large number of secondary electrons produced due to the deflected beam hitting the electrodes and then causing additional undesired ionization events. While we extracting the recoil ions it becomes essential to blank the electron beam. For this purpose, the present experiment with electron impact ionization requires two sets of fast switches, one set for switching electron beam and the other for switching of pusher and puller simultaneously. By using commercial off the shelf power MOSFETs we built fast switches to achieve this. Very commonly used fast single output switches are detailed in few literature for various applications [21–24]. Dual output fast pulsers for time-of-flight mass spectrometry are also available commercially, but are quite expensive generally.

It is necessary to have a pair of switches which can operate in a synchronized manner to switch the pusher and puller plates in the spectrometer which enables us to control the extraction cycle accurately. We use a pair of fast power MOSFETs triggered in synchronism to achieve this. A brief schematic of the high voltage MOSFET switch circuit is as shown in **Figure 3**. In order to minimize the probability of damage to the external TTL pulse generator due to noise produced by the high

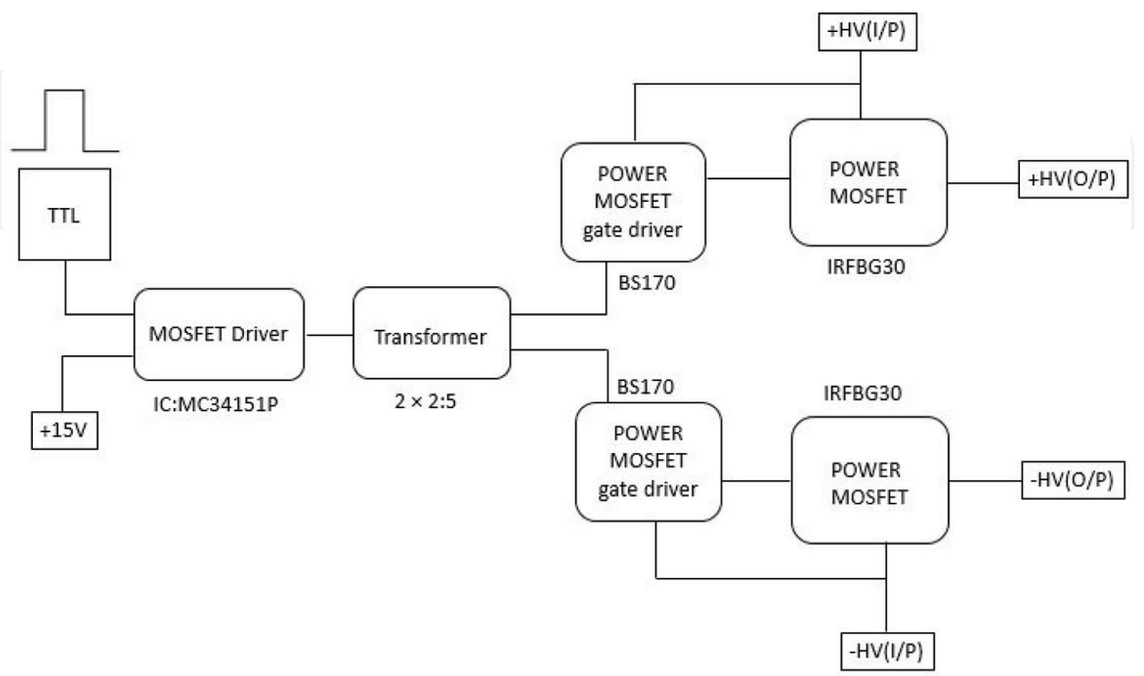

Figure 3.
Schematic of high voltage MOSFET switch (push-pull).

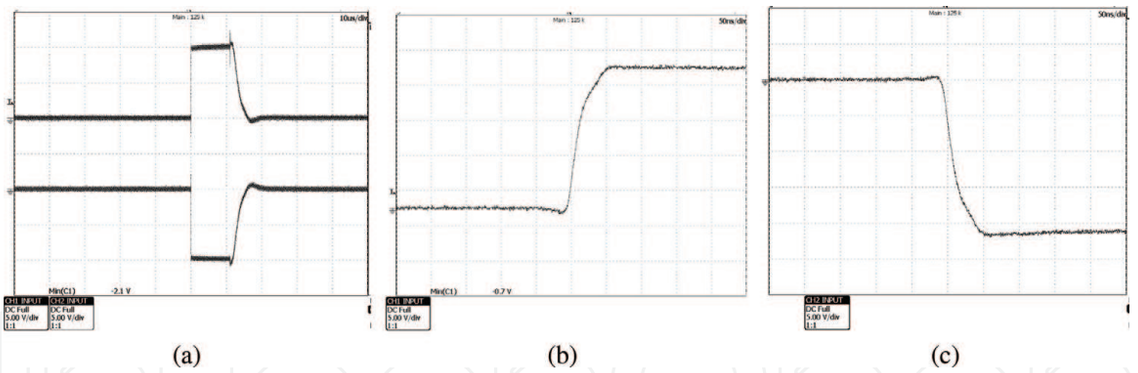

Figure 4.
High voltage MOSFET switch output (a) push-pull mode, (b) rise time (<50nS) in push mode, (c) fall time (<50nS) in pull mode.

voltage section of the circuit, the TTL pulse is passed through several logic gates. This pulse is then used to trigger a MOSFET driver (IC31415P) and the output of the driver is fed to a toroidal transformer with single primary (two turns) and a pair of secondary (five turns each). Gate of the main power MOSFET is controlled by each of the two outputs, triggers a pair of small signal MOSFETs (BS170) which in turn control the. We have tested the switch with voltages as high as ±300 V and could achieve rise/fall times of less than 50 ns with load (shown in **Figure 4b, c**). **Figure 4a** shows the fall/rise time at the end of the pulse was about 5 μs (note push-pull mode fall time) and was not necessary to improve as it played no role in the measurement.

A pair of deflectors and an aperture in between are used to achieve the electron beam pulsing. A single output MOSFET switch is used for one of the deflectors closer to the electron gun and this switch was derived from the same circuit described above but by using only one branch and using a cascade of four identical MOSFETs to achieve pulsing ability for voltages as high as ±2000 V.

4. Simulation

For optimized geometry as well as voltages for ion trajectory (as shown in **Figure 5a**, we performed the Simulation of our time-of-flight mass spectrometer with SIMION8.0 [25]. We simulated conditions with as much as 2.5 mm

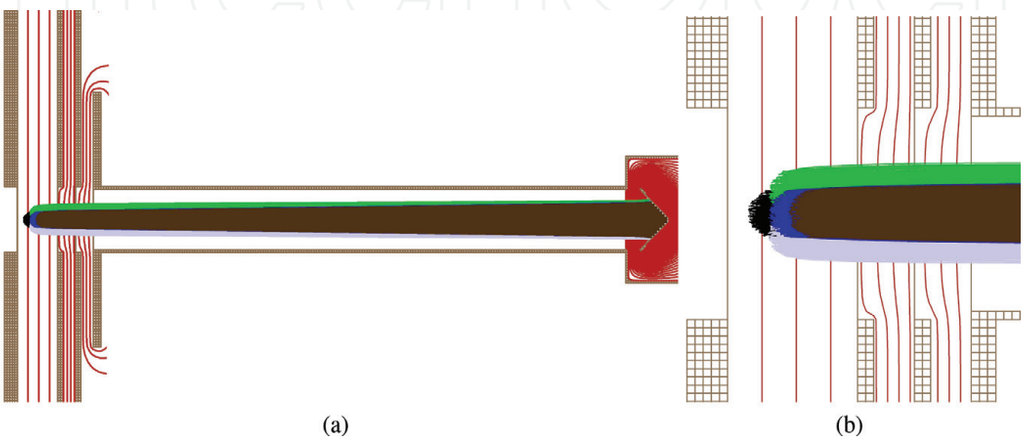

Figure 5.
(a) Trajectory simulated for naphthalene ($C_{10}H_8$) with 480 μm/μs velocity from different position (colored as blue, green, black, white, brown) in the interaction region (b) Particle distribution in the interaction region. Red contours are the equipotential lines.

displacement of the center of the interaction region along the ToF axis as well as in the direction perpendicular to the ToF axis (**Figure 5b**). From our simulation the collection efficiency is estimated by assuming a spherical distribution of the source of diameter 6 mm and assuming an rms velocity twice as large as the value of 300 K that is 480 μm/μs is as the worst case scenario and in all the cases, we could achieve 100% collection efficiency. The electron beam is pulsed with a width of 500 ns. By using deflector blank pulsing method the pulse rise and fall times of 50 ns was obtained, where we pulse the deflector just before the first aperture and hence the electron pulse was effectively on for about 400 ns. The molecular ion extraction field (i.e., pusher-puller plates) is pulsed to 125 V/cm to extract the ions immediately after electron beam pulse is deflected off. The pusher-puller pulse are delayed for delayed extraction of molecular ions, for various delay times with reference to the electron beam pulse. From our calculation 99.9% of the naphthalene intact ions are expected to have thermal velocities less than 480 μm/μs at room temperature and this implies that they can move only 2.5 mm in 5 μs, as our simulations gave us the freedom of shifting the source position of the naphthalene target over the range of 2.5 mm. Thus, we have considered 5 microseconds as the maximum value of our delayed extraction time. The effect of the rise time of the extraction voltage to the molecular velocity spread is numerically calculated, which is 20 μm/μs for naphthalene molecule. So by taking into consideration the spread in thermal velocity, as well as the field effect for naphthalene molecule, the total spread in the velocity is expected to be a maximum of 500 μm/μs. In this case also we could achieve collection efficiency of 100% as per our simulation.

5. Result and discussions

Various projectile electron beam energy values with varying amounts of delay between the electron pulse-off and extraction pulse-on time are used for recording the Naphthalene mass spectra. The mass spectra obtained at different beam energies, as well as extraction delays, are systematically normalized to the single ionization peak area. For comparison between different beam energies and delay combinations, the area of each individual peak after such normalization could directly be considered.

A typical mass spectra is dominated by singly ionized naphthalene molecule followed by prominent peaks originating due to acetylene evaporation losses, as well as intact di-cation, and di-cation with $H_2/2H_2$ loss as shown in **Figure 6**. There are several energetic fragmentation channels are also visible but are not as prominent. The intensity of single C loss and minimal intensity of 3C loss are hardly seen. The single ionization peak is preceded by one or two H atom loss is in general. The mass spectra reported here is not discernible due to our modest resolution. The possible loss of multiple H along with acetylene loss is negligible as shown in the acetylene loss region. On the other hand, the diacetylene loss region, shows two clear peaks due to loss of C_4H_2 and C_4H_4 and the latter could be due to the sequential loss of two acetylene molecules. Significantly, the peak following mass at 64 mass units can be assigned clearly to the di-cation. The formation of exactly half mass fragment for naphthalene is highly improbable unless it is accompanied by several other peaks due to the concurrent loss of multiple H atoms and that would cause a large spread in the mass spectra. A dominant $2H/H_2$ loss channel is observed with about 50% of the di-cation peak intensity and a fast evaporation of neutral 2H or H_2 and hence a large internal energy deposition due to low impact parameter collision is indicated distinct appearance of such a peak. We could ignore safely the 2H loss channel as it is observed to be less likely in previous investigations as

demonstrated by Jochims et al. [8] and thus unless stated explicitly otherwise, we will only refer to H_2 loss possibility wherever the loss of 2 mass units is concerned. The effect is even stronger in the case of di-cation that a large peak is observed at 51 mass units coming from di-cation of naphthalene with the loss of one acetylenes and the acetylene loss competes with H loss in the case of single ionization. Similarly, this peak is again accompanied by H_2 loss along with acetylene loss. As shown earlier in ion-PAH collisions studies [4, 6] we see the dominant H_2 channel. It is $C_3H_3^+$ and $C_3H_4^+$ that dominate the spectra and the rest largely come as by-products of various decay channels in the mass region near 39 units.

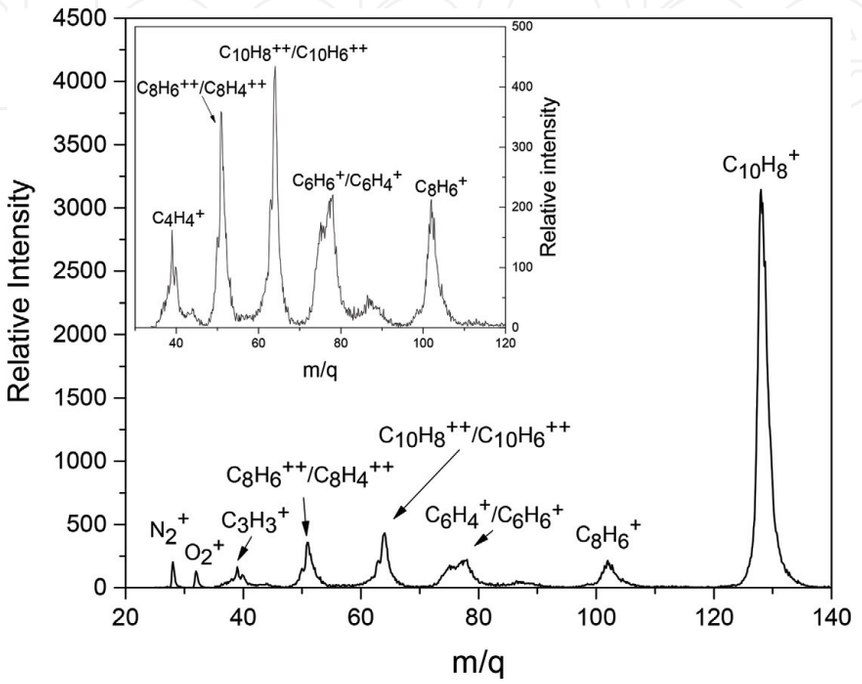

Figure 6.
The mass spectrum of naphthalene($C_{10}H_8$) at 1000 eV electron impact (Inset: naphthalene fragments).

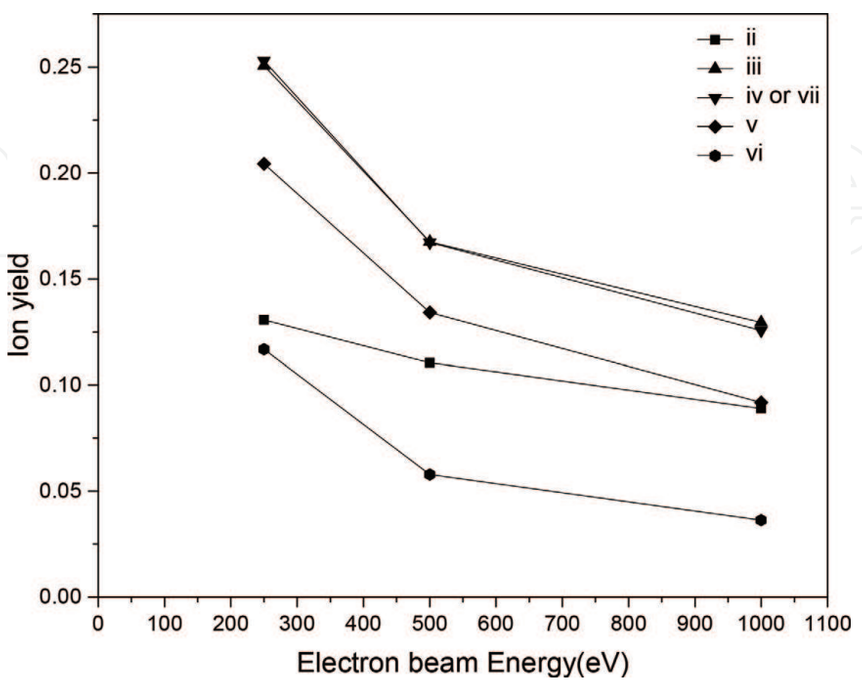

Figure 7.
Projectile electron beam energy dependence of different decay channel with zero delay time extraction. Decay channels are labeled as listed above.

For low-Z targets like hydrocarbons, the projectile energy dependence of the electron impact ionization process is very commonly known to peak at about 70–100 eV and at higher energy, the cross section varies as $\ln E/E$. Interestingly, the acetylene loss channel that shows a distinctly different behavior, as seen from **Figure 7** except that all the channels considered here follow a similar trend.

Thus, we have considered the following decay channels for our analysis.

i. $$C_{10}H_8 + e^- \rightarrow C_{10}H_8^+ + 2e^-$$

ii. $$C_{10}H_8 + e^- \rightarrow C_8H_6^+ + C_2H_2 + 2e^-$$

iii. $$C_{10}H_8 + e^- \rightarrow C_8H_5^+ + C_2H_2 + H + 2e^-$$

iv. $$C_{10}H_8 + e^- \rightarrow C_6H_6^+ + C_4H_2 + 2e^-$$

v. $$C_{10}H_8 + e^- \rightarrow C_6H_5^+ + C_2H_2 + C_2H + 2e^-$$

vi. $$C_{10}H_8 + e^- \rightarrow C_6H_4^+ + C_4H_4(2 \times C_2H_2) + 2e^-$$

vii. $$C_{10}H_8 + e^- \rightarrow C_5H_3^+ + C_2H_2 + C_3H_3 + 2e^-$$

viii. $$C_{10}H_8 + e^- \rightarrow C_4H_4^+ + C_4H_2 + C_2H_2 + 2e^-$$

ix. $$C_{10}H_8 + e^- \rightarrow C_4H_3^+ + 2 \times C_2H_2 + C_2H + 2e^-$$

x. $$C_{10}H_8 + e^- \rightarrow C_4H_2^+ + 3 \times C_2H_2 + 2e^-$$

xi. $$C_{10}H_8 + e^- \rightarrow C_3H_3^+ + C_3H_3 + C_4H_2 + 2e^-$$

xii. $$C_{10}H_8 + e^- \rightarrow C_{10}H_8^{++} + 3e^-$$

xiii. $$C_{10}H_8 + e^- \rightarrow C_{10}H_6^{++} + 2H/H_2 + 3e^-$$

xiv. $$C_{10}H_8 + e^- \rightarrow C_8H_6^{++} + C_2H_2 + 3e^-$$

xv. $$C_{10}H_8 + e^- \rightarrow C_8H_4^{++} + C_2H_2 + 2H/H_2 + 3e^-$$

The loss of one or more H atom from the intact mono-cation is not shown explicitly in the list but is one of the most important channels. As observed by Gotkis et al., the primary decay channel for naphthalene is either H loss or acetylene

loss [12]. It should be noted that the loss of multiple H and acetylene fragments are the prominent statistical decay modes for PAHs and therefore they can be very useful in understanding the dynamics of the internal degrees of freedom in PAHs. Acetylene loss is clearly the most useful channel to study from the data we present here. Higher order ionizations like double and triple ionization are low impact parameter processes and thus a detailed direct coulomb interaction model is more relevant in such cases. In this study our main goal is to explore the plasmon excitation which is a large impact parameter process and it is known to produce singly charged cations for the case of PAHs [26]. We expect strong dynamical and statistical effects in the singly charged naphthalene ions and the associated evaporation products like single and double acetylene loss in our case. Various decay channels are referred in the manuscript according to the numbers given in the list above.

Jochims et al. are discussed the reaction sequence for acetylene loss and the formation of phenyl-acetylene $C_8H_6^+$ from $C_{10}H_8$ in detail [26]. An intermediate is formed by the breaking of the transannular bond accompanied by the migration of H in the naphthalene cation and this is followed by the successive cleavage of C-C bond with a loss of C_2H_2 molecule and the formation of polyacetylene cation [26].

The first six decay channels are considered here with mono-cations and the rest may come from very energetic mono-cation or di-cation. Thus the processes governing the production of the latter decay channels can be treated as low impact parameter and high internal energy channels. And subsequently these decay channels are expected to have substantially large decay rates compared to the decay rates for mono-cations leading to decay channels ii and iii. This unique behavior is evident as shown in **Figure 8a–c** in which plot the relative intensity of all the decay channels at 250, 500 and 1000 eV electron impact energies. The very first clear observation is that the decay channels ii evolve very differently compared to the rest of the channels as a function of extraction delay and this can be seen in **Figure 9a, b**. The diacetylene loss channel show an increase in the yield fraction followed by a steady population or a slight decrease up to 5 μs extraction delay on the other hand, the last five decay channels show a clear decrease from the zero delay onwards. This decay behaviors indicates that the last five reactions have decay rates that are much larger than 10^6 and assuming these arise from the statistical dissociation.

The interaction energy for the formation of larger sized fragments according to reactions iv - viii needs to be well above 22 eV as discussed by Ruhl et al. [18]. The plasmon excitation is expected to peak at about 17 eV [26]. In the data for each beam energy, we observe that compared to the acetylene loss the decay channel iii peak shows a faster rate of change and this can be understood from the fact that the decay rate of channel iii is marginally higher than that of the acetylene loss channel. Interestingly we see a gradual decrease in the relative intensity of all the daughter channels as a function of projectile energy. We can assign two major possibly for the decay channel iii: [1] neutral acetylene evaporation from mono-cation and [2] the dissociation of $C_4H_2^+$ fragment. Moreover, this could also be the C_4H_n fragment but it is not resolved well in our spectra. The population of evaporative products grows substantially in earlier times and after about 3 μs, it starts to drop again and behavior is seen even at 500 and 1000 eV beam energies. This suggesting that the first increase comes due to plasmon excitation and reduces its contribution as we go to higher beam energies and this observation is in complete agreement with the behavior seen in decay channel ii. On the other hand, the rest of the channels, show gradual and continuous decrease in yield with extraction delay time. In the case of decay channel ii, the scales are longer than that for channel ii is seen. The decay channel iv to viii represents more energetic processes and hence show a decrease in

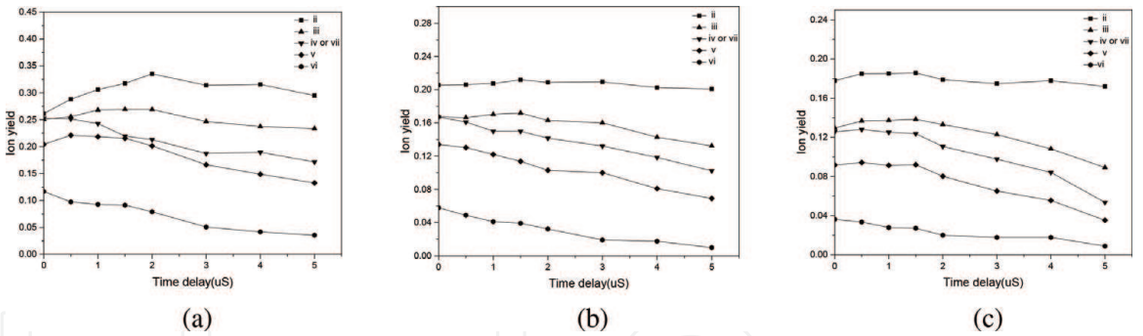

Figure 8.
Various fragmentation channels of naphthalene at (a) 250 eV, (b) 500 eV, (c) 1000 eV electron impact energies. Decay channels are labeled as listed above.

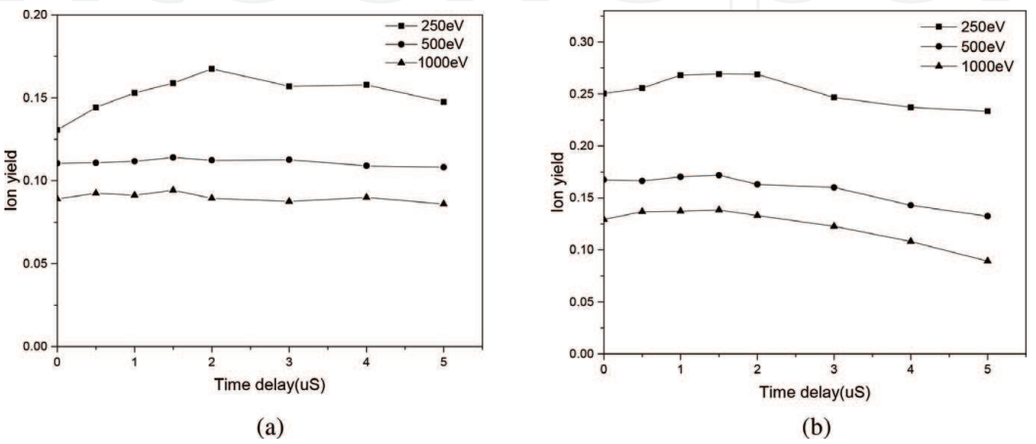

Figure 9.
(a) Decay channel ii (C_2H_2 Loss) and (b) decay channel iii (C_4H_2 or $2 \times C_2H_2$ loss) at various electron impact energies.

population fraction. These channels from the zero delay time, indicating sufficiently fast decay accompanied by sufficient kinetic energy release to cause fast dispersion of daughter ions from the interaction volume.

6. Conclusion

For PAHs in general and for naphthalene in particular a strong influence of the plasmon resonance excitation is known to be present. This effect has recently gained importance due to its possible role in the formation of molecular hydrogen and acetylene molecules in ISM and has been under investigation using far-UV photo-excitation as well as heavy ion-induced excitation. In this work, we have shown the effect of plasmon excitation under by high energy electron impact excitation. The time evolution of the acetylene evaporation, which is known to be a by-product of the plasmon excitation process, is measured for this study. A pulsed electron source along with the pulsed extraction of recoil ions using fast high voltage pulses is implemented and varying the extraction delay we observe the parent and daughter ion yields of naphthalene molecule is observed.

The most dominant low energy channels commensurating with the excitation energy, in range of 7–8 eV leading to a total energy loss of 15–16 eV range is the decay channels leading to loss of acetylene and the loss of diacetylene. Acetylene loss shows much weaker energy dependence compared to the other channels which again is a well-known property of plasmon excitation. In the case of acetylene evaporation processes the time scales of few microseconds are seen and yields of

acetylene evaporation population grow by about 20% as the delay is varied from 0 to 5 μs. Importantly, this work demonstrates that the relatively simple and well-known technique of delayed extraction time-of-flight mass spectrometry can be very useful in certain circumstances like broader energy loss mechanisms i. e, plasmon excitation in charged particle interaction with PAHs. The time evolution of a group of statistical decay channels that could otherwise be inaccessible due to the large range of decay constants can be probed using this unique technique.

Author details

Najeeb Punnakayathil
Department of Physics, Stockholm University, Stockholm, Sweden

*Address all correspondence to: najeeb.punnakayathil@fysik.su.se

References

[1] Salama F, Allamandola LJ. Electronic absorption spectroscopy of matrix-isolated polycyclic aromatic hydrocarbon cations. i. the naphthalene cation ($C_{10}H^{+}_{8}$). The Journal of Chemical Physics. 1991;**94**(11): 6964-6977

[2] Lessen D, Freivogel P, Maier JP. Laboratory evidence for highly unsaturated hydrocarbons as carriers of some of the diffuse interstellar bands. Nature. 1993;**366**(6454):439-441

[3] Postma J, Bari S, Hoekstra R, Tielens AGGM, Schlathölter T. Ionization and fragmentation of anthracene upon interaction with kev protons and particles. The Astrophysical Journal. 2010;**708**(1):435

[4] Mishra PM, Rajput J, Safvan CP, Vig S, Kadhane U. Electron emission and electron transfer processes in proton-naphthalene collisions at intermediate velocities. Physical Review A. 2013;**88**: 052707

[5] Kadhane U, Misra D, Singh YP, Tribedi LC. Effect of collective response on electron capture and excitation in collisions of highly charged ions with fullerenes. Physical Review Letters. 2003;**90**:093401

[6] Reitsma G, Zettergren H, Boschman L, Bodewits E, Hoekstra R, et al. Ion-polycyclic aromatic hydrocarbon collisions: Kinetic energy releases for specific fragmentation channels. Journal of Physics B: Atomic, Molecular and Optical Physics. 2013;**46**(24):245201

[7] Mishra PM, Avaldi L, Bolognesi P, Prince KC, Richter R, Kadhane UR. Valence shell photoelectron spectroscopy of pyrene and fluorene: Photon energy dependence in the far-ultraviolet region. The Journal of Physical Chemistry A. 2014;**118**(17): 3128-3135

[8] Jochims H, Baumgärtel H, Leach S. Structure-dependent photostability of polycyclic aromatic hydrocarbon cations: Laboratory studies and astrophysical implications. The Astrophysical Journal. 1999;**512**(1):500

[9] Boschi R, Clar E, Schmidt W. Photoelectron spectra of polynuclear aromatics. iii. The effect of nonplanarity in sterically overcrowded aromatic hydrocarbons. The Journal of Chemical Physics. 1974;**60**(11):4406-4418

[10] Schmidt W. Photoelectron spectra of polynuclear aromatics. v. correlations with ultraviolet absorption spectra in the catacondensed series. The Journal of Chemical Physics. 1977;**66**(2): 828-845

[11] Alagia M, Candori P, Falcinelli S, Pirani F, Mundim MSP, Richter R, et al. Dissociative double photoionization of benzene molecules in the 26–33 ev energy range. Physical Chemistry Chemical Physics. 2011;**13**(18): 8245-8250

[12] Gotkis Y, Oleinikova M, Naor M, Lifshitz C. Time-dependent mass spectra and breakdown graphs. 17. naphthalene and phenanthrene. The Journal of Physical Chemistry. 1993; **97**(47):12282-12290

[13] Linstrom PJ, Mallard WG. NIST Chemistry WebBook, NIST Standard Reference Database Number 69. Vol. 20899. Gaithersburg, MD: National Institute of Standards and Technology; 2016

[14] Deutsch H, Margreiter D, Märk T. A semi-empirical approach to the calculation of absolute inner-shell electron impact ionization cross sections. Zeitschrift für Physik D Atoms, Molecules and Clusters. 1994; **29**(1):31-37

[15] Kim Y-K, Rudd ME. Binary-encounter-dipole model for electron-impact ionization. Physical Review A. 1994;**50**:3954-3967

[16] Vallance C, Harland PW, Maclagan RG. Quantum mechanical calculation of maximum electron impact single ionization cross sections for the inert gases and small molecules. The Journal of Physical Chemistry. 1996;**100**(37): 15021-15026

[17] Hwang W, Kim Y-K, Rudd ME. New model for electron-impact ionization cross sections of molecules. The Journal of Chemical Physics. 1996; **104**(8):2956-2966

[18] Ruehl E, Price SD, Leach S. Single and double photoionization processes in naphthalene between 8 and 35 ev. The Journal of Physical Chemistry. 1989; **93**(17):6312-6321

[19] Van Brunt RJ, Wacks ME. Electron-impact studies of aromatic hydrocarbons. iii. Azulene and naphthalene. The Journal of Chemical Physics. 1964;**41**(10):3195-3199

[20] Wiley WC, McLaren IH. Time-of-flight mass spectrometer with improved resolution. Review of Scientific Instruments. 1955;**26**(1150):39-441

[21] Baker R, Johnson B. Series operation of power mosfets for high-speed, high-voltage switching applications. Review of Scientific Instruments. 1993;**64**(6): 1655-1656

[22] Jiang W. Fast high voltage switching using stacked mosfets. IEEE Transactions on Dielectrics and Electrical Insulation. 2007;**14**(4): 947-950

[23] Chappell P, Campden K. Switching performance of power mosfets with capacitive loads at high frequency and high voltage for square wave generators. Measurement Science and Technology. 1992;**3**(4):356

[24] Bernius MT, Chutjian A. High-voltage, full-floating 10-mhz square-wave generator with phase control. Review of Scientific Instruments. 1989; **60**(4):779-782

[25] Dahl D. Simion 3D Version 6.0. In: 43rd ASMS Conference on Mass Spectrometry and Allied Topics; Atlanta, Ga; 1995. p. 717

[26] Jochims H, Rasekh H, Rühl E, Baumgärtel H, Leach S. The photofragmentation of naphthalene and azulene monocations in the energy range 7–22 ev. Chemical Physics. 1992; **168**(1):159-184